

Dependance of weak localization cone with the photons brownian Doppler shift

Max Lesaffre, Michael Atlan and Michel Gross*

Laboratoire Kastler Brossel de L'Ecole Normale Supérieure UMR 8552 CNRS, 24 rue Lhomond F-75005 Paris

(Dated: September 14, 2021)

We report the first observation of the dependence of the coherent backscattering (CBS) enhanced cone with the frequency of the backscattered photon. The experiment is performed on a diffusing liquid suspension and the Doppler broadening of light is induced by the brownian motion of the scatterers. Heterodyne detection on a CCD camera is used to measure the complex field (i.e. the hologram) of the light that is backscattered at a given frequency. The analysis of the holograms yield the frequency and the propagation direction of the backscattered photons. We observe that the angular CBS cone becomes more narrow in the tail of the brownian spectrum. The experimental results are in good agreement with a simple theoretical model.

PACS numbers: 42.25.Dd, 42.25.Hz, 71.55.Jv

DOI: 10.1103/PhysRevLett.97.033901

Coherent backscattering (CBS) of light is a photon self interference effect which leads to an enhanced intensity cone in the backscattering direction. This effect, which is related to the solid state physics phenomenon of weak Anderson localization, has been extensively studied both experimentally and theoretically. Since the first observation of CBS from colloidal suspension [1, 2], the phenomenon has been observed on many experimental systems such as powders [3, 4, 5], liquid crystals [6], photonic crystals [7], and cold atoms gases [8, 9, 10, 11]. The CBS effect has also been studied on acoustic [12, 13, 14] and seismic waves [15].

In most of the CBS experiments done in the optical domain, the angular distribution of the backscattered light is measured by using an incoherent detection method. The signal that is detected by a photomultiplier, a photodiode or a CCD camera is proportional to the optical field intensity. In this letter we propose to study the CBS effect more precisely by using a coherent detection method [16]. The backscattered field is summed with a coherent reference field in order to detect the interference pattern of the two fields. The detection is thus sensitive to the phase of the backscattered field.

In this letter, we propose a detection scheme for the CBS effect, which involves a heterodyne detection of the light on a 2D detector (CCD camera). Since the pixel to pixel relative phase of the detected backscattered field is accurately measured, we record the digital hologram of the field [17]. By adjusting the frequency of the heterodyne detection local oscillator, we are able to precisely select the frequency of the backscattered field that is detected. We are thus able to measure the backscattered light average intensity as a function of both the propagation direction (as done commonly) and the frequency i.e. as a function of both the wave vector direction $\mathbf{k}/|\mathbf{k}|$ and the modulus $|\mathbf{k}|$. The CBS effect can then be observed

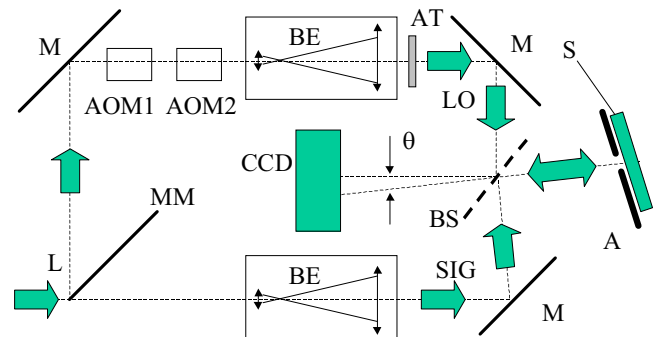


FIG. 1: Experimental Setup. L: main laser, MM: moving mirror, M: mirror, LO and SIG: local oscillator and signal arms, BE: beam expander, AT: attenuator, AOM1, AOM2: acousto optic modulators, BS: beam splitter, S: cell filled with the diffusing suspension, A: rectangular aperture, CCD: CCD camera.

with a backscattered field whose frequency is shifted with respect to the incident incoming field. Since this shift is a Doppler shift which is related to the motion of the scatterers, we can study the influence of the motion of the scatterers on the CBS signal. We will see in particular that the angular width (and more generally the angular shape) of the enhanced backscattered cone depends on the frequency offset.

Fig 1 shows the experimental setup. The 780 nm, 50 mW beam of the laser L (Sanyo DL-7140-201, current: 95 mA) is split in two beams LO and SIG, which are both vertically linearly polarized. The main beam SIG (> 90% of the power, frequency ν_L) illuminates the diffusing sample S (7 cm high \times 8 cm width \times 1 cm depth cell which is filled with a pure or a diluted intralipid suspension: Endolipide 20%; B. Braun Medical SA, diffusion anisotropy factor $g = 0.65$ at $\lambda = 780\text{nm}$ [18]). To detect the S backscattered light signal, the LO beam (< 10% of the power) is mixed to the signal beam with the beam splitter BS. The LO + SIG interference pattern (or heterodyne beat) is recorded by a CCD camera (PCO Pixelfly: 12 bits, $\nu_{CCD} = 12.5$ Hz exposure time 20 ms

*Electronic address: gross@lkb.ens.fr

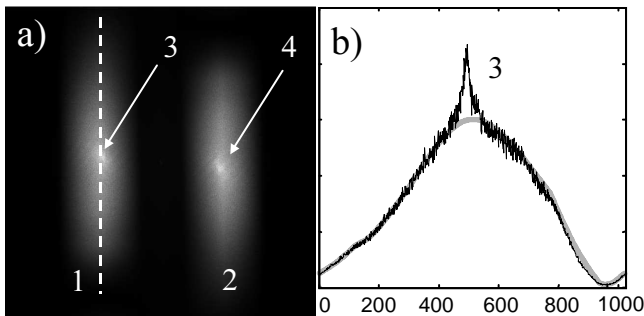


FIG. 2: A) Linear scale 1024×1024 calculated image of the average k-space field intensity $|\tilde{E}|^2$ for $\nu_{LO} = \nu_L$. One pixel is 1.13×10^{-4} radian. B) Cut of the image along the dashed line (black curve). Angular gain of the experiment (solid grey line).

with 1280×1024 pixels of $6.7 \times 6.7 \mu\text{m}$) and transferred to a PC computer.

To avoid saturation of the CCD camera the LO beam is attenuated by the attenuator AT. The power is finely adjusted by moving the mirror MM. By using the AOM1 and AOM2 acousto optic modulators (Crystal Technology: $\nu_{AOM1,2} \simeq 80\text{MHz}$), the LO beam frequency ν_{LO} can be freely adjusted: $\nu_{LO} = \nu_L + (\nu_{AOM1} - \nu_{AOM2})$. Two numerical synthesizers with the same 50 MHz quartz reference clock provide the $\nu_{AOM1,2}$ radiofrequency (RF) signals. Two beam expanders BE ($\times 25$: Spectra Physics model 334) enlarge the LO and SIG beams. The BE focus are adjusted to get a plane wave LO beam on the CCD, and a plane SIG illumination beam on the sample.

To get the complex field E at frequency ν , we use the 4-phase heterodyne variant of the phase-shifting method [17, 19]. We record sequences of 4 CCD images I_i at $t_i = t_0 + i/\nu_{CCD}$ with $i = 0..3$. E interferes with the local oscillator field E_{LO} , and $I_i = |E_{LO}e^{j2\pi\nu_{LO}t_i} + Ee^{j2\pi\nu t_i}|^2$ where $j^2 = -1$. We can choose $\nu_{LO} = \nu - \nu_{CCD}/4$, and $|E_{LO}| \gg |E|$. E is then given by the simple 4-phase equation $E = a[(I_0 - I_2) + j(I_1 - I_3)]$ where a is a constant. Due to the motion of the scatterers, the backscattered light frequency spectrum is broad, and the 4-phase equation performs the heterodyne detection on the two sidebands frequencies $\nu^\pm = \nu_{LO} \pm \nu_{CCD}/4$, yielding to the field components $E(\nu^\pm)$. The 4-phase equation should be thus rewritten as: $E(\nu^+) + E^*(\nu^-) = (I_0 - I_2) + j(I_1 - I_3)$ [20]. In the holographic reconstruction, the 2 components $E(\nu^+)$ and $E^*(\nu^-)$ yield to 2 different images corresponding to the holographic grating orders ± 1 , which may spatially overlap. To spatially separate the images, we have (i) reduced the pupil size by using a black rectangular aperture A (1 cm width \times 5 cm high), (ii) moved the sample at a respective distance $D_{sample} \simeq 25$ cm to the CCD, and (iii) shifted the LO beam *off axis* (θ on Fig.1) [21].

We have recorded $N = 256$ series of 4 images ($4 \times N$ images) with the 1 cm thick cell filled with Intralipid

10% (optical depth $\sim 20 l_s^*$ where l_s^* is the transport mean free path). The LO beam is unshifted in frequency (i.e. $\nu_{LO} = \nu_L$), and the CCD acquisition time is 20 ms per image. For each series, we have calculated the real space field $E(x, y)$ by the 4-phases equation, and the k-space field by 2D Fast Fourier Transform (FFT): $\tilde{E}(k_x, k_y) = FFT E(x, y)$. The angular distribution of the field intensity is then obtained by summing $|\tilde{E}|^2$ over the N series of images. Fig.2A) shows the k-space field calculated average intensity $|\tilde{E}|^2$. Calculations are performed on a 1024×1024 matrices obtained from the 1280×1024 CCD raw data after truncation. From now on, we will consider the angular size α_0 of the k-space pixels as the units for the angle. Due to the FFT we have: $\alpha_0 = \lambda/(1024 \times d_{pixel}) = 1.13 \times 10^{-4}$ radian.

The two vertical oblong spots (1,2) seen on Fig.2A are the two grating orders (± 1) images of the sample. Due to the off-axis configuration, images (1) and (2) do not overlap. The images are blurred (the images are oblong while the aperture A is rectangular) since the holographic reconstruction (FFT) is done at infinite distance while the object is located at a finite distance D_{sample} . The (1,2) spots also represent the angular distribution of the backscattered light, and we can see narrow brighter spots (3,4) in the middle of the spots (1,2) that are the CBS enhanced cones. Due to the aperture A and moreover the fact that the sample is quite far away from the CCD, the light, which is backscattered far from the illumination axis, does not reach the CCD. This means that the angular detection efficiency of our setup is not flat (the wide spots 1 and 2 do not fill the k-space). To analyze the shape of the CBS cone, we have made a cut along the vertical line that passes in the center (x_0, y_0) of the CBS white spot (dashed line of Fig.2 A) and we have plotted the CBS signal (black curve of Fig.2 B). To improve the SNR (signal to noise ratio), the plotted curve is obtained by summing over the lines $x = x_0 - 5$ to $x_0 + 5$. The CBS peak (3) is clearly seen, but, as mentioned above, the background is not flat.

We have corrected the signal from the background distortion by using the measured holographic data to calculate the complex field image of the sample in the aperture A plane. From that calculation we got the position of the aperture A i.e. D_{sample} , the shape of the illumination zone, and the local variations of the illumination intensity. To get holographic signal $|\tilde{E}|^2$ that we should obtain if there is no CBS effect (i.e. if the photons are scattered by the sample in all directions with equal probability), we have calculated the blurred intensity image of the objet that is expected with a focusing at infinite distance. We have by this way the expected background signal i.e. the efficiency of our setup for detecting the backscattered light in a given angular direction. This quantity is plotted as a grey solid line on Fig.2B, which agrees with the observed shape of the CBS background.

The heterodyne detection technique allows the study of new physical effects since the frequency of the backscattered light that is detected can be finely adjusted within

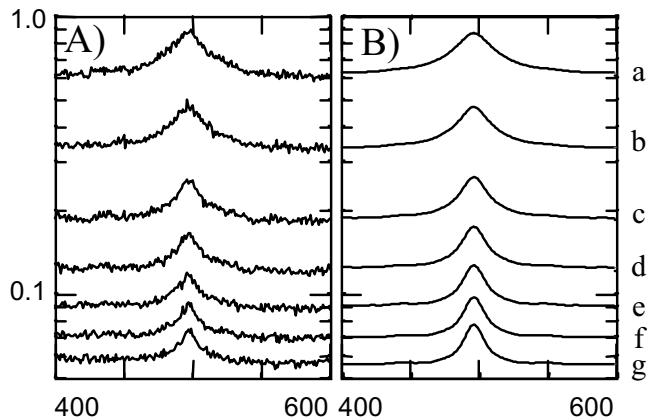


FIG. 3: Angular shapes of the CBS peak for $|\nu_{LO} - \nu_L| = 0$ (a), 100(b), 200(c), 300(d), 400(e), 500(f) and 600 Hz(g). The curves are obtained by summing over the $x = x_0 - 5$ to $x_0 + 5$ lines. To make all curves visible on the same diagram, logarithmic scale is used on the y vertical axis ($y = 0.05$ to 1.0). Horizontal axis is angle (1.13×10^{-4} radian per point). A) Experimental results. B) Theoretical predictions.

the brownian spectrum. We have repeated the previous experiment for different LO frequencies: $\nu_{LO} - \nu_L = +0, +100 \dots +600$ Hz (curve a, b, ...g of Fig.3A). To correct the angular detection efficiency of our setup, the measured signal (solid line of Fig.2B) is divided by the expected background signal (heavy grey line), which is calculated from the $\nu_{LO} = \nu_L$ experimental data, in order to gain the highest SNR (signal to noise ratio) measurement. Fig. 3A shows the CBS cone angular shape obtained by this way. The detection efficiency correction is seen to be efficient and the background is flat. As expected, the CBS cone signal and the background both decrease when $|\nu_{LO} - \nu_L|$ increases (i.e. when the detection is done in the tail of the brownian spectrum). Moreover, one observes a new physical effect, the angular width of the CBS cone also decreases with $|\nu_{LO} - \nu_L|$ (curve a to curve g).

This effect can be understood quite simply. By changing the frequency of the detection (i.e. ν_{LO}), one changes the distribution of travel paths that contribute to the signal. Since each scattering event broadens the photon frequency spectrum, one selects, by pushing ν_{LO} in the tail of the brownian spectrum, travel paths with many scattering events (to get photons far from the center of the brownian spectrum, one needs more scattering events), i.e. longer travel paths. This corresponds to a narrowing of the CBS peak.

To make a quantitative analysis of this effect, we have measured the brownian diffusion constant D_B of the intralipid particules by considering that the CBS background measured on Fig.3A yields the shape of the brownian frequency spectrum. In the case of the backscattering by single diffusor, this spectrum is a Lorentzian of width $4k^2D_B$ [23]. In the multi diffusion case, each travel

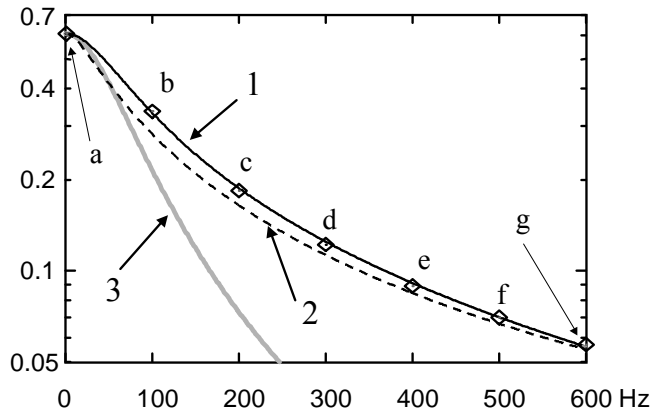


FIG. 4: Frequency spectrum of the backscattered light (logarithmic scale vertical axis). Points are the CBS background measured on curves a to g of Fig.3A. Curve 1 (solid line) is the brownian theoretical shape calculated by Monte Carlo, curve 2 (dashed line) results from [22], curve 3 (solid grey line) is the single scatterer Lorentzian. Horizontal axis is $\nu_{LO} - \nu_L$.

path yields a Lorentzian of width $D_B \Sigma_i |\mathbf{q}_i|^2$ (where Σ_i is the summation over the scattering events i , and $\mathbf{q}_i = \mathbf{k}_i - \mathbf{k}_{i-1}$ is, for each event, the incident versus exiting difference of wavevectors [22]). The spectrum is then a sum of Lorentzians. By considering a set of 10000 travel paths, we have calculated the shape of the multi diffusion spectrum (Fig.4 curve 1). The paths are obtained by simple (scalar approximation, Henyey-Greenstein scattering function) Monte Carlo simulation [24] with $g = 0.65$. The multi diffusion spectrum (curve 1) has been compared with the single scatterer spectrum (curve 3), and with the diffusion wave spectroscopy predictions (curve 2). This one is the Fourier transform of $g_1(t) = e^{-\gamma(6k^2D_B t)^{1/2}}$ [22] with $\gamma = 1.9$ (i.e. for parallel polarisation and $g = 0.65$). We have adjusted the frequency scale to make curves 1 to fit the measured point (a to g). The width of curve 3 ($4k^2D_B = 74$ Hz) yields D_B .

We have used our Monte Carlo set of paths to calculate the angular shape of the CBS cone. For each path, the photons may travel forward (from the first to the last scatterer) or in reverse. The interference of the two paths yield a cosine angular intensity distribution analog to a Young fringe pattern. By summing these fringes over the paths, one gets the CBS enhanced cone. This intuitive idea dates to the CBS original papers [1, 2], and is illustrated by a web java applet [25]. We have generalized this calculation by considering the angular and frequency distribution of light for each path, and then summing over the paths. The CBS curves of Fig.3 correspond to the 2D cuts (angle, frequency) distribution along the $\nu_{LO} - \nu_L = 0, 100, \dots, 600$ Hz lines. We have plotted on Fig.3B the curves that result from the random walk calculation. To make a good theory versus experiment comparison, the Fig.3B curves are obtained by summing over the 11 cuts made on the experimental

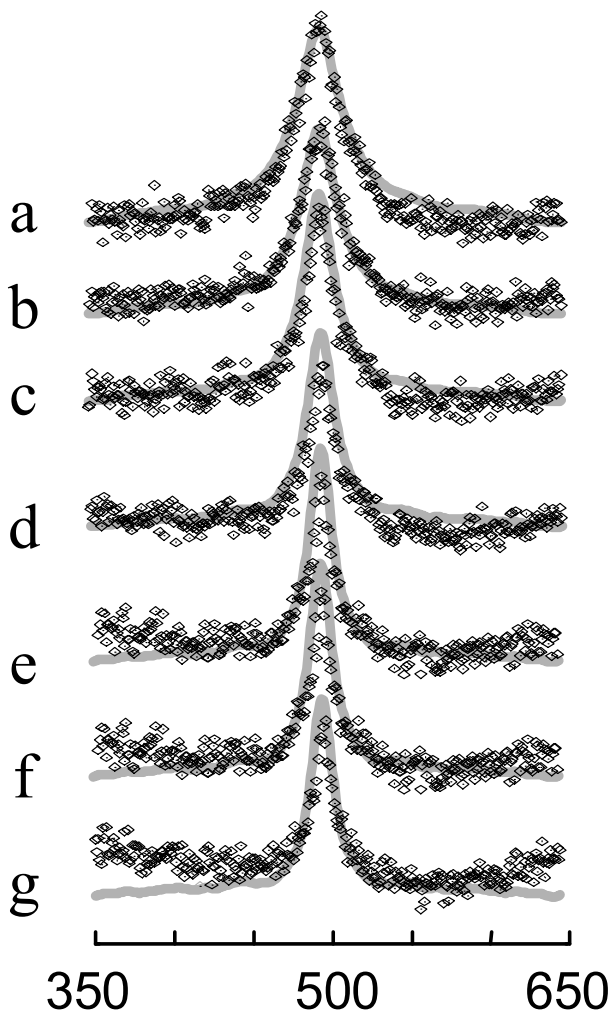


FIG. 5: Same as Fig.3 but with arbitrary units linear scale vertical axis. The points are experimental results, the solid grey curves the theoretical predictions.

data ($x = x_0 - 5$ to $x_0 + 5$). The angular position of the CBS cone, the width of the CBS peak, and the CBS enhanced factor η have been determined from the curve a of Fig.3A ($\nu_{LO} = \nu_L$). The other curves (b to g) are then obtained without any free parameters.

As seen, the experimental results (Fig.3A) are in good agreement with the theoretical predictions (Fig.3B). The CBS enhancement factor ($\eta = 1.48$) is lower than 2 because the linear polarizations are parallel, and because we have summed over 11 parallel lines. With good optical component and careful matching of the BE focus, our system could be diffraction limited by the CCD area. In that case, the angular resolution should exactly be one pixel of the k-space. We have plotted the CBS curves with a linear scale for the vertical axis. For each curve (a to g) the scale is arbitrarily adjusted.

In this letter, we report the first observation of a dependence of the coherent backscattering (CBS) enhanced cone with the frequency of the backscattered photons. The narrowing of the CBS cone that is observed in the tail of the brownian spectrum is in good agreement with a simple model which describes the effect of the travel path distribution. We do not observe any break of reciprocity because the scatterers do not move during the travel of the photon and the scattering cross section does not depend on the motion of the scatterers (as it could do in cold atom experiments [11]). These results are made possible by the development of a new detection method of the backscattered photons, which is based on heterodyne detection of the photons with a CCD camera. This method, which allows the study of both the angular and spectral properties of the backscattered light, opens the way to the observation of new physical effects in disordered systems. The authors thank D. Delande, A. Tourin, J. de Rosny, G. Montambaux and D. Bonn for fruitful discussions. Authors acknowledge also french ANR for its support.

-
- [1] M.P. Van Albada and A. Lagendijk. Observation of weak localization in a random media. *Phys. Rev. Lett.*, 55(24):2692, December 1985.
 - [2] P.-E. Wolf and G. Maret. Weak localization and coherent backscattering of photons in disordered media. *Phys. Rev. Lett.*, 55:2696–2699, December 1985.
 - [3] S. Etemad, R. Thompson, and M. J. Andrejco. Weak localization of photons: Universal fluctuations and ensemble averaging. *Phys. Rev. Lett.*, 57:575–578, 1986.
 - [4] M. Kaveh, M. Rosenbluh, I. Edrei, and I. Freund. Weak localization and light scattering from disordered solids. *Phys. Rev. Lett.*, 57:2049–2052, 1986.
 - [5] D.S. Wiersma, M. P. van Albada, B. A. van Tiggelen, and A. Lagendijk. Experimental evidence for recurrent multiple scattering events of light in disordered media. *Phys. Rev. Lett.*, 74:4193–4196, 1995.
 - [6] D. V. Vlasov, L. A. Zubkov, N. V. Orekhova, and V. P. Romanov. Weak localization due to scattering of light in nonoriented liquid crystals. *JETP Letters*, 48(2):91–94, July 1988.
 - [7] AF Koenderink, M. Megens, G. van Soest, W.L. Vos, and A. Lagendijk. Enhanced backscattering from photonic crystals. *Phys. Lett. A*, 268:104, 2000.
 - [8] G. Labeyrie, F. de Tomasi, J.-C. Bernard, C. A. Müller, C. Miniatura, and R. Kaiser. Coherent backscattering of light by cold atoms. *Phys. Rev. Lett.*, 83:5266–5269, 1999.
 - [9] T. Chanelière, D. Wilkowski, Y. Bidet, R. Kaiser, and C. Miniatura. Saturation-induced coherence loss in coherent backscattering of light. *Phys. Rev. E*, 70:036602, 2004.
 - [10] V. Shatokhin, C. A. Müller, and A. Buchleitner. Coherent inelastic backscattering of intense laser light by cold atoms. *Phys. Rev. Lett.*, 94:043603, 2005.
 - [11] G. Labeyrie, D. Delande, R. Kaiser, and C. Miniatura. Light Transport in Cold Atoms and Thermal Decoher-

- ence. *Physical Review Letters*, 97(1):13004, 2006.
- [12] G. Bayer and T. Niederdränk. Weak localization of acoustic waves in strongly scattering media. *Phys. Rev. Lett.*, 70:3884–3887, 1993.
- [13] A. Tourin, A. Derode, P. Roux, B. A. van Tiggelen, and M. Fink. Time-dependent coherent backscattering of acoustic waves. *Phys. Rev. Lett.*, 79:3637–3639, 1997.
- [14] J. de Rosny, A. Tourin, A. Derode, P. Roux, and M. Fink. Weak localization and time reversal of ultrasound in a rotational flow. *Phys Rev Lett.*, 95(7):074301, Aug 2005.
- [15] E. Larose, L. Margerin, B. A. van Tiggelen, and M. Campillo. Weak localization of seismic waves. *Phys. Rev. Lett.*, 93:048501, 2004.
- [16] M. Pitter, E. Jakeman, and M. Harris. Heterodyne detection of enhanced backscatter. *Optics Letters*, 22(6):393–395, 1997.
- [17] F. LeClerc, L. Collot, and M. Gross. Numerical heterodyne holography using 2d photo-detector arrays. *Opt. Lett.*, 25:716, Mai 2000.
- [18] H. J. van Staveren, C. J. M. Moes, J. van Marle, M. J. C. van Gemert, and S. A. Prahl. Light scattering in Intralipid-10 in the wavelength range of 400-1100 nm. *Appl. Opt.* , 30:4507–4514, November 1991.
- [19] F. LeClerc, M. Gross, and L. Collot. Synthetic-aperture experiment in the visible with on-axis digital heterodyne holography. *Opt. Lett.*, 26:1550–1553, 2001.
- [20] M. Gross, P. Goy, and M. Al-Koussa. Shot-noise detection of ultrasound-tagged photons in ultrasound-modulated optical imaging. *Opt. Lett.*, 28(24):2482–2484, 15 2003.
- [21] U Schnars and W Jueptner. Direct recording of holograms by a ccd target and numerical reconstruction. *J. Opt. Soc. Am. A*, 11(7):2011–2015, 1994.
- [22] D. J. Pine, D. A. Weitz, J. X. Zhu, and E. Herbolzheimer. Diffusing-wave spectroscopy: dynamic light scattering in the multiple scattering limit. *J. Phys. France*, 51:2101–2127, 1990.
- [23] B. J. Berne and R. Pecora. *Dynamic Light Scattering*. John Wiley, New York, 1976.
- [24] S. L. Jacques. Light distributions from point, line and plane sources for photochemical reactions and fluorescence in turbid biological tissues. *Photochem Photobiol*, 67:23–62, 1998.
- [25] http://cops.tnw.utwente.nl/education/5_oc_cohback.html